PHYSICAL REVIEW C **71**, 064308 (2005)

Relativistic mean field study of clustering in light nuclei

P. Arumugam, B. K. Sharma, and S. K. Patra
Institute of Physics, Sachivalaya Marg, Bhubaneswar-751 005, India

Raj K. Gupta*
Department of Physics, Panjab University, Chandigarh-160 014, India
(Received 26 January 2005; published 22 June 2005)

The clustering phenomenon in light, stable and exotic nuclei is studied within the relativistic mean field (RMF) approach. Numerical calculations are done by using the axially deformed harmonic oscillator basis. The calculated nucleon density distributions and deformation parameters are analyzed to look for the cluster configurations. The calculations explain many of the well-established cluster structures in both the ground and intrinsic excited states. Comparisons of our results with other model calculations and the available experimental information suggest that the RMF theory is well suited for studying clustering in light nuclei. A few discrepancies and their possible sources are also discussed.

DOI: 10.1103/PhysRevC.71.064308 PACS number(s): 21.60.Gx, 24.10.Jv

I. INTRODUCTION

Clustering is a very general phenomenon, which appears in atomic, nuclear, subnuclear, and the cosmic worlds [1]. In nuclear dynamics, as seen in light stable nuclei, clustering is one of the essential features and various cluster structures have been known even in the low-energy region. Also, in the physics of unstable nuclei, clustering features comprise one of the central subjects. It is already well known [2–7] that clustering structures appear in the ground states of ordinary light nuclei with $N = Z$ or in their neighbourhood. Even though this phenomenon has now been studied for a long time, many things remain to be learned and some recent experimental activities focus on this subject [8].

When cluster structures are prominent, the description by conventional mean-field models based on the shell-model-like picture becomes insufficient. Fortunately, the properties of light nuclei with cluster structures have been well studied with cluster models where the existence of clusters is assumed *a priori*. This assumption, however, sets a limitation for applying the cluster models to "exotic" (unstable) nuclei, where structural information is rather scanty. Thus, a model that could explain both the mean-field and clustering properties of nuclei would be helpful to obtain a systematic understanding of both the stable and exotic nuclei. Examples of such successful frameworks are the methods of Fermionic molecular dynamics (FMD) [9] and antisymmetrized molecular dynamics (AMD) [6], both of which describe well the structural properties of several nuclei and their excited states, in the lighter mass region [7,10–13].

Another model, argued here in this paper for the first time, that is capable of explaining the clustering shapes in light nuclei is the relativistic mean field theory (RMFT) [14]. This theory has been successfully applied to nuclei throughout the nuclear chart and, with some extensions [15], also to nuclear matter and neutron stars. The success of RMFT in the light-mass regime, however, is limited and several arguments have been put forth to explain the shortcomings. Some arguments could be related to the inadequacy of the mean-field approximation itself, the RMF parameters, the shape degrees of freedom, and the lack of proper pairing correlations. Nevertheless, in the present paper, we explore for the first time the applicability of the RMFT for explaining the possible cluster structures in lighter mass stable and exotic nuclei. Specifically, we have considered here the various $^{6-14}$Be and the odd-mass isotopes of $^{11-19}$B nuclei and the $N = Z\,\alpha$ nuclei from C to S. Since the results of RMFT calculations for most of these nuclei, explaining structural properties other than clustering, are already published (see, e.g. [16–21]), here we discuss only the appearance of cluster states and the versatility of RMFT in this respect. A brief report of this work is given in Ref. [22].

II. THEORETICAL FRAMEWORK

The relativistic mean field approach is well known and the theory is well documented [23–28]. Here we start with the relativistic Lagrangian density for a nucleon-meson many-body system [23,24,26–28]:

$$\begin{aligned}\mathcal{L} = {} & \overline{\psi_i}\{i\gamma^\mu\partial_\mu - M\}\psi_i + \frac{1}{2}\partial^\mu\sigma\,\partial_\mu\sigma - \frac{1}{2}m_\sigma^2\sigma^2 \\ & - \frac{1}{3}g_2\sigma^3 - \frac{1}{4}g_3\sigma^4 - g_s\overline{\psi_i}\psi_i\sigma - \frac{1}{4}\Omega^{\mu\nu}\Omega_{\mu\nu} \\ & + \frac{1}{2}m_w^2 V^\mu V_\mu + \frac{1}{4}c_3(V_\mu V^\mu)^2 - g_w\overline{\psi}_i\gamma^\mu\psi_i V_\mu \\ & - \frac{1}{4}\vec{B}^{\mu\nu}\cdot\vec{B}_{\mu\nu} + \frac{1}{2}m_\rho^2\vec{R}^\mu\cdot\vec{R}_\mu - g_\rho\overline{\psi}_i\gamma^\mu\vec{\tau}\psi_i\vec{R}^\mu \\ & - \frac{1}{4}F^{\mu\nu}F_{\mu\nu} - e\overline{\psi}_i\gamma^\mu\frac{(1-\tau_{3i})}{2}\psi_i A_\mu. \end{aligned} \tag{1}$$

*Presently, DFG Mercator Professor, Frankfurt Institute for Advanced Studies (FIAS), J.-W.-Goethe-Universität, D-60438 Frankfurt am Main, Germany.

 ©2005 The American Physical Society

The field for the σ meson is denoted by σ, that for the ω meson by V_μ, and that for the isovector ρ meson by $\vec{R}_\mu$. A^μ denotes the electromagnetic field. The ψ_i are the Dirac spinors for the nucleons whose third component of isospin is denoted by τ_{3i}. Here g_s, g_w, and g_ρ and $\frac{e^2}{4\pi} = \frac{1}{137}$ are the coupling constants for σ, ω, ρ mesons and photons, respectively. g_2, g_3 and c_3 are the parameters for the nonlinear terms of σ and ω mesons, respectively. M is the mass of the nucleon and m_σ, m_ω, and m_ρ are the masses of the σ, ω, and ρ mesons, respectively. $\Omega^{\mu\nu}$, $\vec{B}^{\mu\nu}$, and $F^{\mu\nu}$ are the field tensors for the V^μ, $\vec{R}^\mu$, and the photon fields, respectively [24].

From the relativistic Lagrangian we obtain the field equations for the nucleons and mesons. These equations are solved by expanding the upper and lower components of the Dirac spinors and the boson fields in a deformed harmonic oscillator basis with an initial deformation. The set of coupled equations is solved numerically by a self-consistent iteration method. The baryon (vector), scalar, isovector, and proton densities are, respectively,

$$\rho(r) = \sum_\alpha \varphi_\alpha^\dagger(r)\varphi_\alpha(r), \tag{2}$$

$$\rho_s(r) = \sum_\alpha \varphi_\alpha^\dagger(r)\beta\varphi_\alpha(r), \tag{3}$$

$$\rho_3(r) = \sum_\alpha \varphi_\alpha^\dagger(r)\tau_3\varphi_\alpha(r), \tag{4}$$

$$\rho_{\rm p}(r) = \sum_\alpha \varphi_\alpha^\dagger(r)\left(\frac{1+\tau_3}{2}\right)\varphi_\alpha(r). \tag{5}$$

The centre-of-mass motion is estimated by the usual harmonic oscillator formula $E_{\rm c.m.} = \frac{3}{4}(41A^{-1/3})$. The quadrupole deformation parameter β_2 is evaluated from the resulting quadrupole moment [24]. The total binding energy and other observables are also obtained by using the standard relations, given in [14,24].

III. DETAILS OF THE CALCULATIONS

In our present calculations, we have used the NL3 parameter set for all the nuclei, except for ^{12}C. The NL3 and NL2 parameter sets do not give proper convergence for the ground state of ^{12}C and hence the next best parameter set NL-SH is used in this case. For lighter mass nuclei, the results of RMF calculations are insensitive to the pairing gap parameter Δ [16], and hence the contribution of pairing is not significant for the chosen light nuclei. This is expected from the small density of states near the Fermi surface for light nuclei. Hence, we present the results of our calculation without considering pairing correlations.

We have solved the mean-field equations self-consistently, taking different inputs of the initial deformation β_0. The quadrupole deformation parameter β_2 is obtained from the calculated quadrupole moments for the protons and neutrons, through

$$Q = Q_n + Q_p = \sqrt{\frac{9}{5\pi}}AR^2\beta_2, \tag{6}$$

where $R = 1.2A^{1/3}$ fm and the Q's are the quadrupole moments. Calculations are done in an axially deformed harmonic oscillator basis with 14 shells, both for bosons as well as fermions. The nuclei considered in the present paper deal with rather large deformed states; even the chainlike structures are known. Also, to get a self-consistently converged solution, one may need a large model space for both the fermions and bosons oscillator shells. For the calculation of these considered nuclei, it is practical to use a reasonably large number for major fermionic and bosonic oscillator shells. This is illustrated in Fig. 1, where we have presented our calculations for ^{32}S with $N_F = N_B = 6$ to 20, in the interval of 2, at the initial deformation of $\beta_2 = 0.7$, using the NL3 parameter set. The physical observables calculated are the total binding energy, rms radii, and the quadrupole deformation parameters, which are plotted in Fig. 1 for various values of the harmonic oscillator quanta $N_{\rm max}$. From the figure it is clear that the solution for ^{32}S converges at $N_F = N_B = 10$. This means that there is no change in results if the number of fermionic and bosonic harmonic oscillator basis is greater than or equal to 10 major shells (i.e., $N_F = N_B \sim 10$). As another example, we have repeated our calculations for ^{16}O at $\beta_0 = 1.5$ and 1.6. In this case, for $N_{\rm max} \leqslant 12$, we could not get the proper solutions. It is evident from the figure that the physical observables remain unaltered with $N_F = N_B = 14$ to 20. Therefore, in the present calculations, we have used $N_F = N_B = 14$ to get a self-consistently converged solution.

As outputs, we obtain different potentials, densities, single-particle energy levels, radii, deformations, and binding energies. For a given nucleus, the maximum binding energy corresponds to the ground state and other solutions are obtained as various excited intrinsic states. For studying the clustering aspects, the densities and deformations are more important. The proton, neutron, and matter densities are obtained in the positive quadrant of the plane parallel to the symmetry axis. Because we choose z axis as the symmetry axis, the densities are evaluated in the $z\rho$ plane, where $x = y = \rho$. Because the space reflection symmetry about z-axis, as well as the ρ axis, is conserved in our formalism, the results obtained in the positive quadrant are suitably reflected in other quadrants, giving a complete picture in the $z\rho$ plane. Such unbroken symmetries of our numerical procedure lead to several limitations, which we discuss in the last section.

IV. RESULTS

As already mentioned in the Introduction, RMF calculations for the various properties of light-mass nuclei have been exhaustively performed by many authors (see, e.g., Refs. [16–21]). However, only a few calculations of the deformations and binding energies are reported [16] where the cluster states are speculated to be present at higher deformations. Here we utilize, for the first time, the density distributions for studying explicitly the cluster states in both the ground and excited states of light nuclei, shown in Figs. 2–10 as filled contour plots. All the density contours presented here are given in boxes of width 20 fm and height

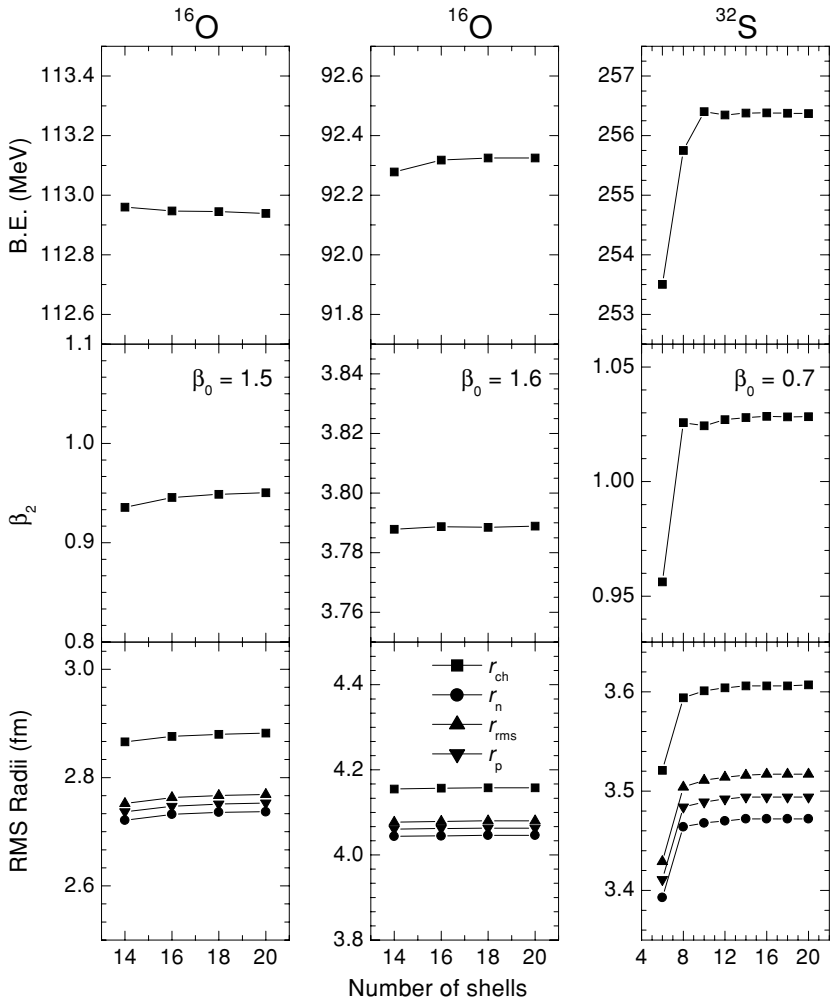

FIG. 1. The RMF results with various values of bosonic (N_B) and fermionic (N_F) major shells. The binding energy, rms radii, and total quadrupole deformation parameter are plotted.

18 fm. A uniform contour spacing of 0.01 fm^{-3} is used for proton and neutron densities, whereas the spacing is 0.02 fm^{-3} for the total density. Full black contours correspond to maximum density and full white ones correspond to zero-density regions. In the following, we present our results first for the Be and B isotopes and then for the α nuclei.

A. Be isotopes

The α-α cluster structure is expected to be well pronounced in the ^{8}Be nucleus. Consequently, the calculation of the spatial distribution of nuclear density in this case will serve as a benchmark of the formalism to explain the cluster structure in light nuclei. The results of our calculation for even-N Be isotopes are given in Fig. 2. The contour plots of neutron, proton ,and total nuclear densities are given in the first, second, and third columns, respectively. We notice clear evidence for the α-α structure in ^{8}Be. The two distinct shaded areas in the figure for ^{8}Be represent the concentration of density being split into two parts, which can be related to the α-α structure. This result gives the first justification for an application of the RMF approach to study clustering structure in light nuclei.

The binding energies obtained in the present calculations are compared with the experimental data in Table I, where

TABLE I. Calculated binding energies (B.E.) and deformation parameters (β_2) for the Be and B isotopes, compared with the experimental data.

Nucleus	B.E. (MeV)		β_2 (Theor.)		
	Theor.	Expt.	Neutron	Proton	Total
^{6}Be	31.28	26.92	0.23	1.15	0.84
^{7}Be	40.69	37.60	0.90	1.20	1.07
^{8}Be	52.76	56.50	1.18	1.20	1.19
^{9}Be	58.02	58.16	0.70	0.90	0.79
^{10}Be	64.87	64.98	0.40	0.67	0.51
^{11}Be	67.74	65.48	0.25	0.58	0.37
^{12}Be	71.80	68.65	0.13	0.48	0.25
^{13}Be	72.28	68.55	0.52	0.62	0.55
^{14}Be	74.37	69.91	0.83	0.74	0.80
^{11}B	76.90	76.20	0.20	0.28	0.23
^{13}B	88.85	84.45	0.05	0.17	0.10
^{15}B	92.48	88.19	0.67	0.44	0.59
^{17}B	94.64	89.53	0.69	0.48	0.62
^{19}B	94.73	90.08	0.43	0.39	0.42

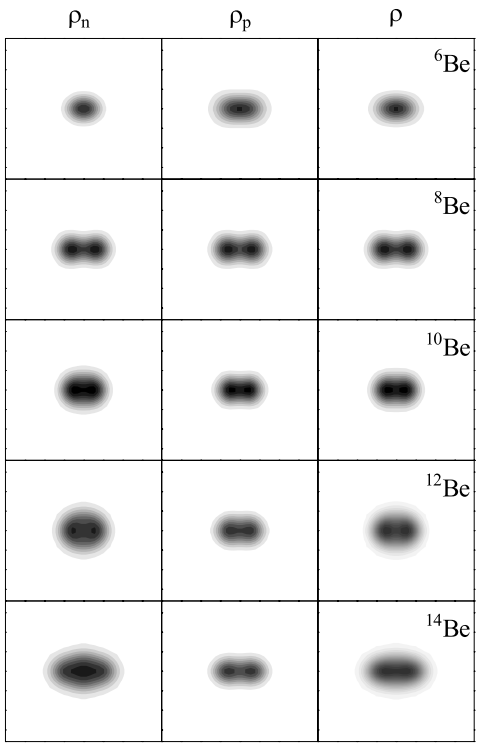

FIG. 2. Contour plot of neutron, proton, and matter density distributions in the even-A isotopes of Be. See text for details about the plotting.

we have presented the corresponding deformations also. To study the variation of the cluster structure with increase or decrease of neutron number, we have examined the internal structure (density distributions) of Be isotopes in Figs. 2 and 3, where Fig. 2 presents our results for even-N Be isotopes and Fig. 3 for odd-N Be isotopes. We have considered here

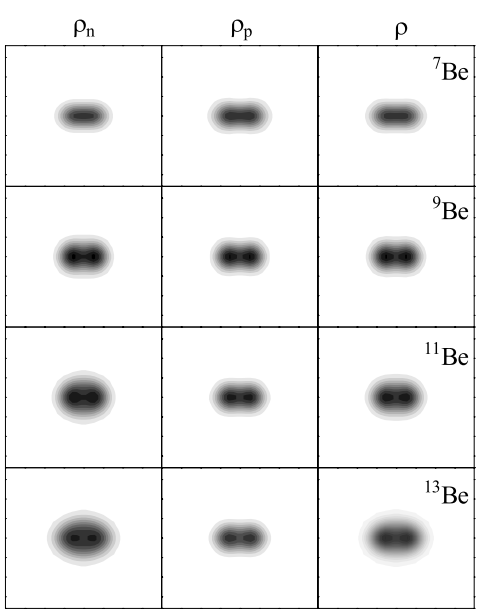

FIG. 3. Same as Fig. 2 but for odd-A isotopes.

the Be isotopes with $6 \leqslant A \leqslant 14$ only. In our calculations, ^{13,14}Be are the drip-line nuclei; a detailed discussion on the stability of these nuclei and the predictions of drip lines in the lighter mass regions based on RMF calculations can be found in Ref. [20]. The density distribution of ^{6}Be in Fig. 2 indicates an $\alpha + 2p$ structure since nuclear matter is more concentrated in the central region. In other calculations (see, e.g. [11]), ^{6}Be is found to have an $\alpha +$ diproton structure, which is forbidden in our calculations because of the assumption of space-reflection symmetry and the lack of parity projection. For the same reason, the more standard prediction of an $\alpha + {}^{3}$He structure in ^{7}Be does not show up in our results in Fig. 3. Also, the ^{7}Be results do not suggest any clear cluster structure in comparison to other nuclei, though we can infer that the protons fall into two groups. As the neutron concentration increases, for Be-nuclei, which are heavier than ^{8}Be, we find that the clustering in proton matter remains almost undisturbed. Thus, we can say that the α-α structure of the core persists with the addition of neutrons to the α-α nucleus ^{8}Be. Furthermore, we notice from the density distributions of protons that the α clusters for ^{9,10}Be are more closely packed, as compared to other cases. The smallest distance between two α clusters occurs for ^{10}Be. Some authors [29] have interpreted this character to be due to the strong pairing effects. Further interpretations of this feature can be found in Refs. [30], which treat the clustering in heavier ($A \geqslant 9$) Be and B isotopes on the same footing as dimers in molecular physics. The variation of the distance between the two α clusters and the corresponding excited states could be related to the nature of the bond (σ, π bonds). The AMD calculations [6,7,11] also discuss such results.

As we go to still heavier isotopes of Be, we notice in Figs. 2 and 3 that another interesting "halo" structure feature develops for ^{13,14}Be. In the case of ^{13}Be, the proton and neutron distributions show that the α-α structure remains intact while the remaining neutrons stay around. In ^{14}Be, from the neutron distribution, we can see that a few more neutrons stick to the α-α core and hence the halo should comprise fewer neutrons (<6 in this case). From the intensity variation in the plots of neutron densities, one could observe that the neutron concentration is not evenly spread from the inner to the outer parts. Hence, one can conjecture that the outer part is not a thick skin of neutrons but a halo with much fewer neutrons. In general, the Be isotopes have an $\alpha + \alpha + xn$ structure, with $\alpha + \alpha$ as the core. The remaining x neutrons are rather sparsely distributed around the core and constitute a "halo" for these heavier isotopes of Be.

Figures 2 and 3 also illustrate the variation of deformations of nuclei with the addition of neutrons. Starting from a well-creviced (necked) prolate shape in ^{8}Be, the deformation gradually decreases and the shape becomes almost spherical in ^{12}Be. Then, a further increase in neutron number induces prolate deformed shapes in ^{13,14}Be, but now the shapes are not creviced. This result is also supported by our calculated deformations in Table I, which agree qualitatively with the predictions of Ref. [6], though our calculated values are somewhat larger. Table I also shows that our calculated binding energies match the experiments within a few million electron volts.

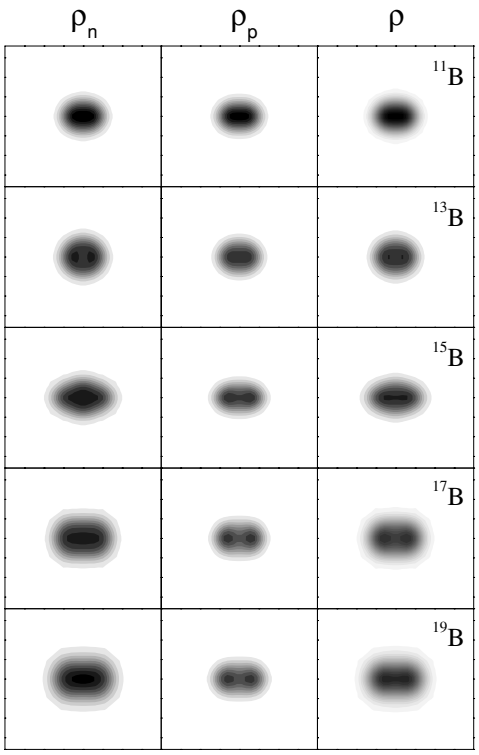

FIG. 4. Contour plot of neutron, proton, and matter density distributions in selected odd-A isotopes of B.

B. B isotopes

The investigations of B isotopes reveal the variation of clustering structure in the presence of one odd proton added to the nucleons contributing to the α-α structure. Here we discuss only the odd-A Boron isotopes and our results are shown in Fig. 4. The ^{15,17,19}B nuclei are weakly bound [20] and ^{19}B is the drip-line nucleus in the B isotopic series. In ^{11}B, we see a halolike structure. However, careful observation of the proton and neutron densities reveals that they are almost distributed in the same space. Hence the outer part of ^{11}B originates from a tail of neutron and proton densities. The creviced α-α structure in the core develops in ^{13}B and remains intact up to ^{19}B. Comparing the results of B and Be isotopes, we see that the 8 neutrons in ^{12}Be and ^{13}B are distributed in a very similar way with distinctly separated parts. Similarly, the 10 neutrons in ^{14}Be and ^{15}B are distributed in the same way but without any distinct clustering. The overall structure can be considered as $\alpha + \alpha + p + xn$, with $\alpha + \alpha + p$ as the core. The sparsely distributed x neutrons form a halo in ^{17,19}B but in ^{11}B they may confined to the skinlike tail.

C. α nuclei

Cluster structures comprising α particles are also expected to be present in the $4N$ α nuclei. Subsequently, the α nuclei could also manifest themselves as clusters in the relatively heavier nuclei. Furthermore, different cluster structures become apparent as the excitation energy in the nucleus increases. This statement [2] includes some rather unusual shapes for a nucleus, including the extreme "chains" of α particles. In this section we present our results for the lighter $4N$ nuclei up to ^{32}S and look for possible α-particle or α-nucleus clustering.

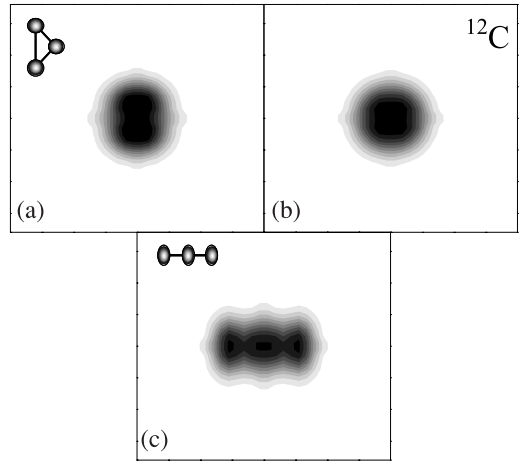

FIG. 5. Matter density distribution in ^{12}C.

For a systematic study of the intrinsic excited states, which differ in deformation, one has to construct the potential energy surfaces with respect to deformation and look for different local minima. Such a calculation for lighter mass nuclei can be found in Ref. [19], where the quadrupole moments are constrained to give different deformations. In the present work, as the deformations encountered are very large, getting self-consistently converged solutions at points other than the local minima is difficult. Hence, instead of performing the quadrupole moment constrained calculations, here we tune the initial guess for deformation (β_0) to obtain solutions at different local minima.

It is known that the persistence or breaking of α clustering is influenced by the spin-orbit interaction (see, e.g. [31,32]). Because the spin-orbit interaction is stronger in heavier mass nuclei, one does not expect these nuclei to be α nucleus-like. Our calculations for ^{208}Pb and ^{304}120 (not shown here) support this argument since we could not see any distinct clustering in these nuclei. It is to be noted here that the spin-orbit interaction is naturally taken care in the RMF theory through the Dirac formalism. A new non-α-nucleus clustering could occur in heavy nuclei (see, e.g. [33]), such as the exotic ^{14}C clustering in radioactive nuclei [34]. Some authors [35] think of possible clustering, such as the fullerenes, even in super-heavy excited compound systems, produced in, say, ^{244}Cm + ^{244}Cm reaction, where these clusters could be the ones belonging to the center island of superheavy elements.

1. ^{12}C

Figure 5 shows our results for ^{12}C, where we obtain three different solutions. The ground state is oblate shaped and coexists with a spherical shape [see Figs. 5(a) and (b) and Table II, where the corresponding deformations and binding energies are given]. The excited state solution exhibits a high prolate deformation. The ground state of ^{12}C has

TABLE II. Calculated binding energies and deformation parameters for the α nuclei from ^{12}C to ^{32}S, along with the experimental data. The probable interpretation for the structures obtained from the theoretically calculated density distributions are also shown, along with the references where similar structures were predicted earlier. Some of the structures proposed are rather speculative owing to the symmetry conservation and other limitations involved in our calculations. In such cases our predictions are given in parentheses.

Nucleus	B.E. (MeV)		β_2		Probable structure	Similar predictions
	Theor.	Expt.	Theor.	Expt.		
^{12}C	89.74	92.16	–0.29	0.58	3α—equilateral triangle	[5,6,10,36]
	89.63		0.00		spherical	
	72.55		2.33		3α—linear chain	[3]
^{16}O	128.84	127.62	0.00		4α—tetrahedron	[5,10,37]
	112.95		0.95		4α—kite	[36]
	92.28		3.79		4α—linear chain	[3]
^{20}Ne	156.70	160.64	0.54	0.73	5α—trigonal bipyramid	[5,7,37]
	151.96		–0.24		^{10}B + ^{10}B	
	108.24		7.76		^{10}B + ^{10}B—(fragments)	
^{24}Mg	194.37	198.26	0.50	0.61	^{12}C + ^{12}C—(central bishpenoid)	[5]
	186.82		–0.26		^{12}C + ^{12}C—trigonal biprism	
^{28}Si	232.08	236.54	–0.34	0.41	D_{3d} symmetry	[5]
	231.18		0.00		hollow sphere—(pentagonal bipyramid)	
	224.11		0.60		^{12}C + α + ^{12}C—trigonal biprism	[5,13,37]
^{32}S	265.96	271.78	0.25	0.31	^{16}O + ^{16}O—(kite)	
	256.38		1.03		^{16}O + ^{16}O—(tetrahedron)	

been universally associated with an equilateral triangle, the 3α-particle structure. This naturally leads to an oblate shape, which our RMF calculations in Table II also support. The density distribution in the $z\rho$ plane shows a smooth variation of density from the center to the periphery. However, the clusters will be distinctly seen only in the plane perpendicular to the symmetry axis. Also, in a two-dimensional calculation of Ref. [36], the α clusters do not show up distinctly. At the higher deformation $\beta = 2.33$, the 3α-chain structure clearly shows up in our calculation presented in Fig. 5(c). This structure is also well reproduced by many other calculations (e.g., Ref. [3]), though it is far from clear as to which state the 3α chain might be connected [4].

2. ^{16}O

Being a doubly magic nucleus, ^{16}O is spherical in shape. Owing to clustering, the density distribution in this nucleus becomes inhomogeneous. Our results, shown in Fig. 6(a), depict hollowness at the center. This means that in a three-dimensional configuration, the four α particles in ^{16}O form a regular tetrahedron. This is our ground state of ^{16}O. The two-dimensional configuration could be of a square, rhombic (or diamond), or kite structure. Similar to other calculations [36], our RMF calculations give a kite structure, shown in Fig. 6(b). This is a highly deformed shape with $\beta = 0.95$ (see Table II). Finally, at the highest deformation $\beta = 3.79$, the RMF solution yields the linear 4α-chain structure for ^{16}O, which is well depicted in Fig. 6(c).

3. ^{20}Ne

The ground state of ^{20}Ne comes is a trigonal bipyramid in our RMF calculations, as is clearly seen in Fig. 7(a). This result agrees well with previous predictions [5,7,37]. The search for the next solution yielded an oblate configuration with $\beta = -0.24$. The corresponding density distribution is as shown in Fig. 7(b). The structure depicted in Fig. 7(b), showing two equally split portions, could not be related to the α-particle clustering of the type seen previously for ^{12}C and ^{16}O. The only possibility is the ^{10}B + ^{10}B configuration, which requires the breaking of one α particle. Note that ^{10}B is the most stable isotope of the observed B nuclei. The work of Ref. [7] also shows that, in the case of ^{20}Ne, the parity asymmetric

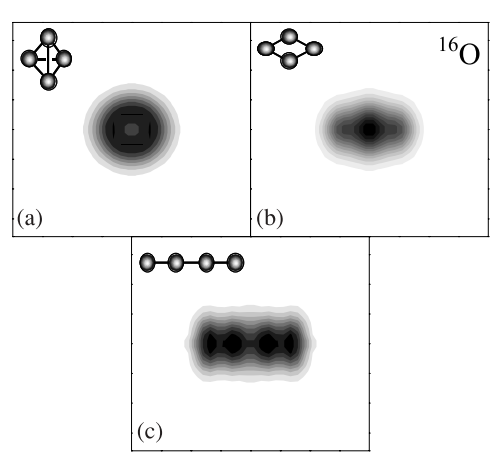

FIG. 6. Matter density distribution in ^{16}O.

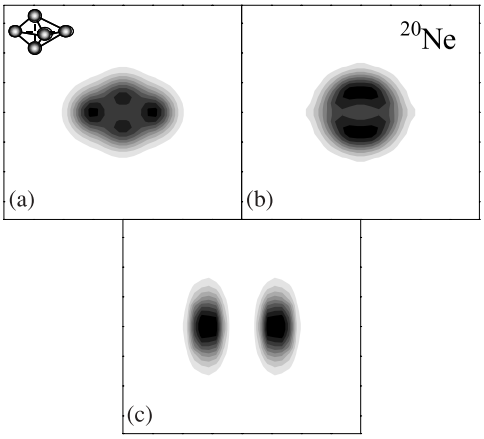

FIG. 7. Matter density distribution in ^{20}Ne.

structures are rather favored. Because we are not performing any parity projection here, such shapes could not be accounted for in our calculations. Finally, the RMF calculations at the next higher deformation gives a stable solution at $\beta = 7.76$. Figure 7(c) shows that this corresponds to a configuration of two completely separated fragments of equal size (possibly two ^{10}B nuclei). Any further increase in energy or deformation will also give the same two fragments, though more separated. It has to be noted that the harmonic oscillator basis expansion may be insufficient at very high deformation, especially for fissioning shapes. Hence, we could not obtain the linear 5α-chain structure in ^{20}Ne, which some experimental studies claim for this nucleus [4].

4. ^{24}Mg

The ^{24}Mg nucleus has been of central interest in clustering studies. Several local minima in the potential energy surface of ^{24}Mg were predicted by Nilsson-Strutinsky calculations made long ago [38], and the corresponding cluster structures for stable deformed configurations were analyzed in detail using the cranked cluster model [39]. Most of the calculations (see e.g. Refs. [37,39]) predict the ground state of ^{24}Mg as a α-^{16}O-α structure with $\beta \sim 0.6$ and having triaxiality [38]. Because our present framework does not support triaxial shapes, we get a different ground-state solution with $\beta = 0.50$ (All the calculations in the present work are done assuming axial symmetry and hence this limits the prediction of a triaxial configuration.) Also, the internal structure (the clustering pattern) obtained in our RMF calculations is different, as shown in Fig. 8(a). Our calculations predict a pattern close

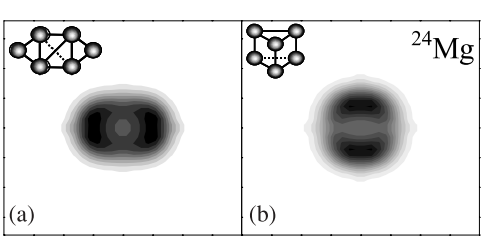

FIG. 8. Matter density distribution in ^{24}Mg.

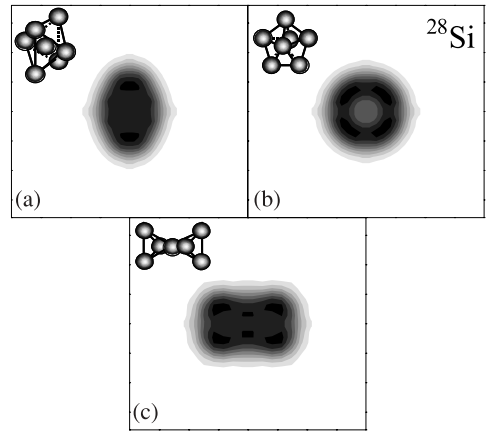

FIG. 9. Matter density distribution in ^{28}Si.

to the central bisphenoid [5], a combination of two ^{12}C nuclei leading to prolate deformation. As we see the density distribution only in the $z\rho$ plane, where the complete structure could not be viewed, the structure assigned here is rather speculative. The first intrinsic excited-state solution from our calculation is shown in Fig. 8(b). This is an oblate shape and can be associated with a ^{12}C + ^{12}C structure where the overlap is parallel to the plane containing the three α particles in each ^{12}C. Hence, in ^{24}Mg both states have the ^{12}C + ^{12}C structure, though with different orientations, one prolate (central bisphenoid) and another oblate (trigonal biprism).

5. ^{28}Si

The ground-state deformation of ^{28}Si is obtained as $\beta = -0.34$. This oblate shape could be associated with the D_{3d} symmetry of crystalline structure or a trigonal biprism with an α particle at the center, as illustrated in Fig. 9(a). Similar to the case of ^{12}C, the distinct clusters could be seen more clearly in the xy plane. The next stable solution in our RMF calculations appear at $\beta = 0.0$, for which the density distribution is shown in Fig. 9(b). This structure with a hollow center could be linked with a pentagonal bipyramid structure, which is known to result normally in an oblate shape [13]. Given that any other combinations of 7α clusters could not give arise to a spherical shape that is hollow at the center, the pentagonal bipyramid could be the best possible, structure where the pentagon may be having a distorted orientation. Finally, we have obtained one more solution with a well-deformed prolate shape ($\beta = 0.6$). The density distribution shown in Fig. 9(c) reveals that this structure is closely related to the D_{3h} symmetry of the crystalline structure or to the ^{12}C-α-^{12}C trigonal biprism [5,13,37].

6. ^{32}S

The ground state of ^{32}S is known to be slightly triaxial [37]. In our calculations the deformation obtained is $\beta = 0.25$ and the density distribution is as shown in Fig. 10(a). One can easily associate the ground state of ^{32}S to an overlapping of two ^{16}O clusters wherein the oxygen clusters have a kitelike structure,

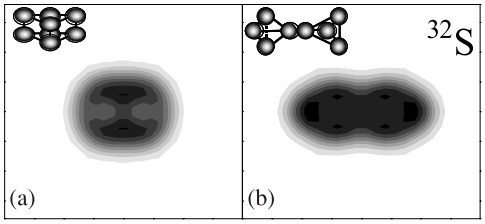

FIG. 10. Matter density distribution in ^{32}S.

finally forming a tetragonal prism. The symmetry of crystalline structure corresponding to this structure is the C_{2v}. The stable solution at a higher deformation is achieved at $\beta = 1.03$. From the density plots in Fig. 10(b), one can infer that this structure also can be linked to a ^{16}O + ^{16}O configuration, though with a different orientation. In this configuration the oxygen clusters are predicted to have a tetragonal structure, similar to what they possess in the ground state. The results of AMD calculations [7] also suggest that the superdeformation in ^{32}S is the same as for the ^{16}O + ^{16}O clustering.

V. SUMMARY AND DISCUSSION

We have seen that the clustering structure of several light-mass nuclei could be well explained by the RMF theory in its present framework. Our results are mostly conform with other theoretical results and experimental information. In Be and B nuclei, our calculations could explain both the α clustering and halo structures. In α nuclei from ^{12}C to ^{32}S, several prominent cluster structures in both the ground and intrinsic excited states could be well described by the RMF calculations. Also, most of the structures could be linked to the standard crystalline structures.

However, several structures could not be explained. For example, in our calculations, the linear α chain could not be obtained for nuclei beyond ^{16}O. Study of these structures requires calculations at large deformations, and our chosen oscillator basis expansion may not be proper at such asymptotic limits. One indication of this behavior is evident from the monotonic increase of binding energy at larger deformations. Calculations in deformed coordinate space may solve some of these issues and will throw more light on the clustering aspects of light nuclei. The neglect of odd multipole shape degrees of freedom or the corresponding space reflection symmetry imposes further serious limitations in explaining nuclei with odd number of particles. For Be and B isotopes, most of the shapes are found to be parity asymmetric in the calculations of Refs. [7,11,12]. Hence, our results for these cases are only qualitative. For ^{24}Mg and ^{32}S nuclei, triaxial shapes have a role to play, and these are not incorporated in our calculations, and may alter the binding energies as well as the ground state and other excited states (local minima). As a consequence, we may get an entirely different solution with a different clustering pattern. The clustering pattern is not distinctively visible in the $z\rho$ plane for ^{12}C and ^{28}Si nuclei, suggesting the requirement of calculations in three dimensions.

Apart from this set of issues, which are related more to numerical techniques, some other facts also limit the success of RMFT for the lighter mass nuclei, as has been already mentioned in the Introduction. Some hints about it could be drawn from the discrepancies in calculated binding energies, listed in Tables I and II. The limitations of mean-field models in the low-mass region could be interpreted as the breakdown of the mean-field approximation itself for few-particle systems that might not have saturated. Simple mean-field models like the phenomenological independent particle model could not explain the clustering features. Because the RMFT comprises finer details of the meson fields, it could explain well the clustering in the lower mass region. For instance, the cluster structures in ground states of ^{8}Be, ^{20}Ne, and ^{28}Si are well explained by our RMF calculations, in spite of the large discrepancies in predicted binding energies. An improvement of the RMFT parameters, with special attention paid to the lighter mass nuclei, has been suggested in Ref. [40].

In spite of all the difficulties just listed, the RMFT could explain successfully many cluster states in light nuclei. The RMF model used here can be regarded now as a fundamental tool of its kind as it explains a variety of phenomena throughout the known nuclear chart and beyond. Over time, extensions of RMFT have fetched rich gains in explaining different phenomenon. For example, halo structures were well explained with the inclusion of pairing correlations with in the Hartree-Bogoliubov framework [41]. Incorporating cranking and correlations such as the random phase approximation could throw more light on the excited states of nuclei. By utilizing effective field theory techniques with the addition of new couplings, the RMFT could be made applicable to nuclear matter and neutron stars [15]. The excited states of cluster configurations are well understood as resonance states and a wealth of experimental data is available. Employing the projection techniques in RMFT could provide access to those excited sates. Nevertheless, the present study demonstrates the applicability of RMFT for studying the clustering phenomenon and provides the scope for understanding in detail the nuclear structure in various regimes while highlighting the versatility of the RMF models.

[1] W. Greiner, Z. Phys. A **349**, 315 (1994).
[2] K. Ikeda, N. Takigawa, and H. Horiuchi, Suppl. Prog. Phys., 464 (1969).
[3] H. Horiuchi, K. Ikeda, and Y. Suzuki, Prog. Theor. Phys. Suppl. **52**, 89 (1972).
[4] M. Freer and A. C. Merchant, J. Phys. G **23**, 261 (1997).
[5] B. R. Fulton, Contemporary Phys. **40**, 299 (1999).
[6] Y. Kanada-En'Yo and H. Horiuchi, Prog. Theor. Phys. Suppl. **142**, 205 (2001).

[7] Y. Kanada-En'Yo, M. Kimura, and H. Horiuchi, C. R. Phys. **4**, 497 (2003).
[8] C. Beck, Int. J. Mod. Phys. E **13**, 9 (2004); and references therein.
[9] H. Feldmeier and J. Schnack, Rev. Mod. Phys. **72**, 655 (2000).
[10] T. Neff and H. Feldmeier, Arxiv:nucl-th/0312130 (2003); and references therein.
[11] Y. Kanada-En'yo, H. Horiuchi, and A. Ono, Phys. Rev. C **52**, 628 (1995).
[12] Y. Kanada-En'yo and H. Horiuchi, Phys. Rev. C **52**, 647 (1995).
[13] Y. Kanada-En'Yo, in *Proceedings of the 8th International Conference on Clustering Aspects of Nuclear Structure and Dynamics*, Nara, Japan, 2003, to be published in Nucl. Phys. A, Arxiv:nucl-th/0409056 (2004).
[14] S. K. Patra, C.-L. Wu, C. R. Praharaj, and R. K. Gupta, Nucl. Phys. **A651**, 117 (1999).
[15] P. Arumugam, B. K. Sharma, P. K. Sahu, S. K. Patra, T. Sil, M. Centelles, and X. Viñas, Phys. Lett. **B601**, 51 (2004).
[16] S. K. Patra and C. R. Praharaj, Nucl. Phys. **A565**, 442 (1993).
[17] S. K. Patra, Nucl. Phys. **A559**, 173 (1993).
[18] A. Bhagwat, Y. K. Gambhir, and S. H. Patil, Eur. Phys. J. A **8**, 511 (2000).
[19] M. S. Mehta, T. K. Jha, S. K. Patra, and R. K. Gupta, Prãmana, J. Phys. **62**, 841 (2004).
[20] T. K. Jha, M. S. Mehta, S. K. Patra, B. K. Raj, and R. K. Gupta, Prãmana, J. Phys. **61**, 517 (2003).
[21] S. K. Patra, R. K. Gupta, and W. Greiner, Int. J. Mod. Phys. E **6**, 641 (1997).
[22] P. Arumugam, S. K. Patra, and R. K. Gupta, in *Proceedings of the DAE-BRNS Symposium on Nuclear Physics, Varanasi (India), December 6–10, 2004* [Board of Research in Nuclear Science (BRNS), Department of Atomic Energy (DAE), Govt. of India, Mumbai, 2004] Vol. 47 B, p. 72.
[23] B. D. Serot and J. D. Walecka, Adv. Nucl. Phys. **16**, 1 (1986).
[24] Y. K. Gambhir, P. Ring, and A. Thimet, Ann. Phys. (NY) **198**, 132 (1990).
[25] C. E. Price and G. E. Walker, Phys. Rev. C **36**, 354 (1987).
[26] Y. Sugahara and H. Toki, Nucl. Phys. **A579**, 557 (1994).
[27] P. K. Panda, S. K. Patra, J. Reinhardt, J. A. Maruhn, H. Stöcker, and W. Greiner, Int. J. Mod. Phys. E **6**, 307 (1997).
[28] S. Gmuca, Nucl. Phys. **A547**, 447 (1992).
[29] M. Seya, M. Kohno, and S. Nagata, Prog. Theor. Phys. **65**, 204 (1981).
[30] W. von Oertzen, Prog. Theor. Phys. Suppl. **146**, 169 (2002); Nuovo Cimento A **110**, 895 (1997).
[31] N. Itagaki, S. Okabe, and K. Ikeda, Prog. Theor. Phys. Suppl. **142**, 297 (2001).
[32] H. Ohta, K. Yabana, and T. Nakatsukasa, arXiv: nucl-th/0404081.
[33] J. Cseh, R. K. Gupta, and W. Scheid, Phys. Lett. **B299**, 205 (1993).
[34] R. K. Gupta and W. Greiner, Int. J. Mod. Phys. **E 3**, 335 (1994, Suppl).
[35] W. Greiner [Private communication to one of us (RKG)].
[36] J. Zhang and W. D. M. Rae, Nucl. Phys. **A564**, 252 (1993).
[37] J. Zhang W. D. M. Rae, and A. C. Merchant, Nucl. Phys. **A575**, 61 (1994).
[38] G. Leander and S. E. Larsson, Nucl. Phys. **A239**, 93 (1975).
[39] S. Marsh and W. D. M. Rae, Phys. Lett. **B180**, 185 (1986).
[40] B. K. Sharma, P. Arumugam, and S. K. Patra, (in preparation).
[41] J. Meng and P. Ring, Phys. Rev. Lett. **77**, 3963 (1996).